doi.org/10.26434/chemrxiv.12671069.v1

Phase Behavior that Enables Solvent-Free Carbonate-Promoted Furoate Carboxylation

Amy Frankhouser, Matthew Kanan

Submitted date: 18/07/2020 • Posted date: 20/07/2020

Citation information: Frankhouser, Amy; Kanan, Matthew (2020): Phase Behavior that Enables Solvent-Free Carbonate-Promoted Furoate Carboxylation. ChemRxiv. Preprint.
https://doi.org/10.26434/chemrxiv.12671069.v1

A solvent-free transformation that enables production of polyester precursors from inedible biomass proceeds from a heterogeneous reaction mixture containing both solid and molten components. Characterization of the evolution of these component phases over the course of the reaction provides insight relevant to process design and scale-up.

Phase Behavior that Enables Solvent-Free Carbonate-Promoted Furoate Carboxylation

Amy D. Frankhouser and Matthew W. Kanan*

Department of Chemistry, Stanford University, Stanford, California 94305, United States

Abstract

Solvent-free chemistry has been used to streamline synthesis, reduce waste, and access novel reactivity, but the physical nature of the reaction medium in the absence of solvent is often poorly understood. Here we reveal the phase behavior that enables the solvent-free carboxylation reaction in which carbonate, furan-2-carboxylate (furoate), and CO_2 react to form furan-2,5-dicarboxylate ($FDCA^{2-}$). This transformation has no solution-phase analog and can be applied to convert lignocellulose into performance-advantaged plastics. Using *operando* powder X-ray diffraction and thermal analysis to elucidate the temperature- and conversion-dependent phase composition, we find that the reaction medium is a heterogeneous mixture of a ternary eutectic molten phase, solid Cs_2CO_3, and solid Cs_2FDCA. During the reaction, the molten phase and solid Cs_2CO_3 diminish as solid Cs_2FDCA accumulates. These insights are critical for increasing the scale of furoate carboxylation and provide a framework to guide the development of other solvent-free transformations.

Main Text

Solvent-free reactions have been investigated primarily as a means to improve the practicality of conventional solution-phase reactions by reducing waste, accelerating the rate, or simplifying purification.[1-9] The unusual properties of a reaction medium composed of neat reactants also raise the possibility of accessing reactivity that is very difficult or impossible to recapitulate in solution. To this end, we recently showed that carbonate (CO_3^{2-}) can promote C–H carboxylation of very weakly acidic aryl C–H bonds ($pK_a > 35$ in organic solvent) in carefully selected solvent-free alkali salts at elevated temperature.[10-13] By contrast, even under forcing conditions in organic solvent, CO_3^{2-} has been found to be incapable of promoting carboxylation of C–H bonds with $pK_a > 27$.[14] The ability to use a simple, regenerable base such as CO_3^{2-} is essential if carboxylation is to be applied to scalable chemical synthesis. Solvent-free alkali salts unlock this possibility for some targets, but a better understanding of the reaction medium is needed to realize this potential.

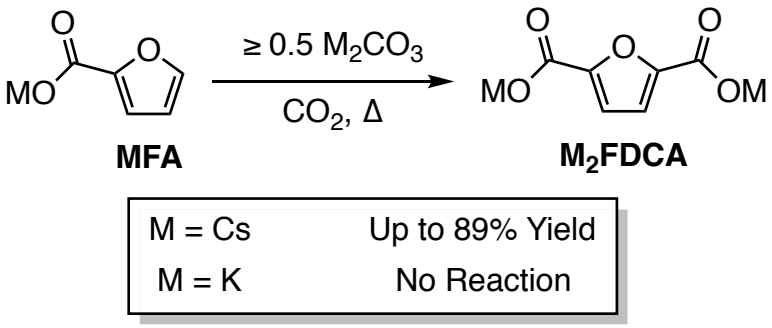

Scheme 1 | Solvent-free carbonate-promoted furoate carboxylation

A promising application of solvent-free CO_3^{2-}-promoted C–H carboxylation is the conversion of furan-2-carboxylate (furoate) into furan-2,5-dicarboxylate ($FDCA^{2-}$) (**Scheme 1**). The protonated form of the carboxylation product – furan-2,5-dicarboxylic acid (FDCA) – is a potential platform chemical for the synthesis of performance-advantaged plastics.[15, 16] Extensive efforts to produce FDCA on a commercial scale from C_6 sugars (glucose and fructose) have been impeded by the technical difficulties and process complexity of dehydrating and oxidizing C_6 sugars.[17] C–H carboxylation opens a new route to FDCA from underutilized C_5 sugar feedstocks (inedible hemicellulose) and avoids many of the process challenges that have plagued C_6 routes.[11]

In its simplest form, furoate carboxylation is performed by combining alkali furoate (MFA) with at least 0.5 equivalents of alkali carbonate and heating the salt mixture under CO_2. Yields of $FDCA^{2-}$ up to 89% have been obtained in laboratory-scale experiments (up to >100 g), but the performance shows a strong dependence on the identity of the alkali cation (**Scheme 1**). When using a single alkali cation, high yields of $FDCA^{2-}$ can be achieved with Cs^+, but no detectable yield is obtained with any of the other alkali cations. Herein, we present a detailed investigation of the physical and structural properties of the reaction mixture components for solvent-free furoate carboxylation. Using a combination of X-ray diffraction and thermal analysis techniques, we elucidate the phase behavior that enables solvent-free furoate carboxylation in Cs^+ salts and explain the lack of reactivity in pure K^+ salts. Our findings reveal how reactivity in this system depends on the phase equilibria that exist within multi-component salt mixtures.

In the solvent-free furoate carboxylation reaction, the material that makes up the reaction medium consists initially of a mixture of alkali furoate (MFA) and alkali carbonate (M_2CO_3). Alkali carbonates are inorganic crystalline solids with high melting points (T_m = 899 °C for M = K; T_m =

793 °C for M = Cs).[18] Hence, any phase behavior that occurs in the mixture at carboxylation temperatures (<280 °C) can be expected to derive primarily from the furoate component. To understand the cation dependence of furoate carboxylation reactivity, we looked first to contrast the structural and thermal properties of potassium and cesium furoate.

Both potassium furoate (KFA) and cesium furoate (CsFA) are crystalline solids at room temperature, though CsFA is distinctly more hygroscopic. A single crystal X-ray structure obtained for KFA shows that the salt packs in the form of 2-dimensional sheets of potassium cations sandwiched between organic anion layers (**Figs. 1a**, **S1**, **S2**). In contrast to KFA, diffraction-quality single crystals of CsFA could not be isolated for determination of a crystal structure, a common problem for aromatic carboxylates.[19] However, ambient temperature synchrotron Powder X-ray Diffraction (PXRD) patterns of anhydrous CsFA indicate that the salt also possesses a layered structure, evidenced by an intense low-index peak. A plausible room temperature structure for CsFA was determined from PXRD data by a simulated annealing procedure[20] after indexing of ambient temperature PXRD patterns for anhydrous CsFA collected at two independent synchrotron beamlines (**Figs. S3–S5**, see **Supporting Information** for additional details). The packing in the resulting structure (**Fig. 1b**) is very similar to that in KFA.

Given the similarity of potassium and cesium furoate at ambient temperature, any differences in the properties of the two salts that are related to their disparity in carboxylation reactivity must manifest only at elevated temperatures. Thermal analysis reveals that the key difference between KFA and CsFA is that only the latter salt can exist as a stable isotropic melt. As with many other alkali carboxylate salts,[21-23] alkali furoates were found to exhibit complex polymorphism. Differential Scanning Calorimetry (DSC) thermograms collected for samples of KFA and CsFA show that upon heating from room temperature, both salts undergo a series of endothermic events prior to the onset of exothermic decomposition (**Fig. 1c,d**). In both cases, the highest temperature endothermic transition was identified as melting (T_m = 390 °C for M = K; T_m = 264 °C for M = Cs), while the lower temperature endothermic events correspond to solid–solid transitions between crystalline or semi-crystalline MFA polymorphs (denoted by Roman numerals increasing with temperature from I for the ambient temperature polymorph). The assignment of these thermal events was further corroborated by Thermogravimetric Analysis, Polarized Optical Microscopy, and Variable Temperature PXRD techniques (**Figs. S6–S11**). Importantly, while the melting

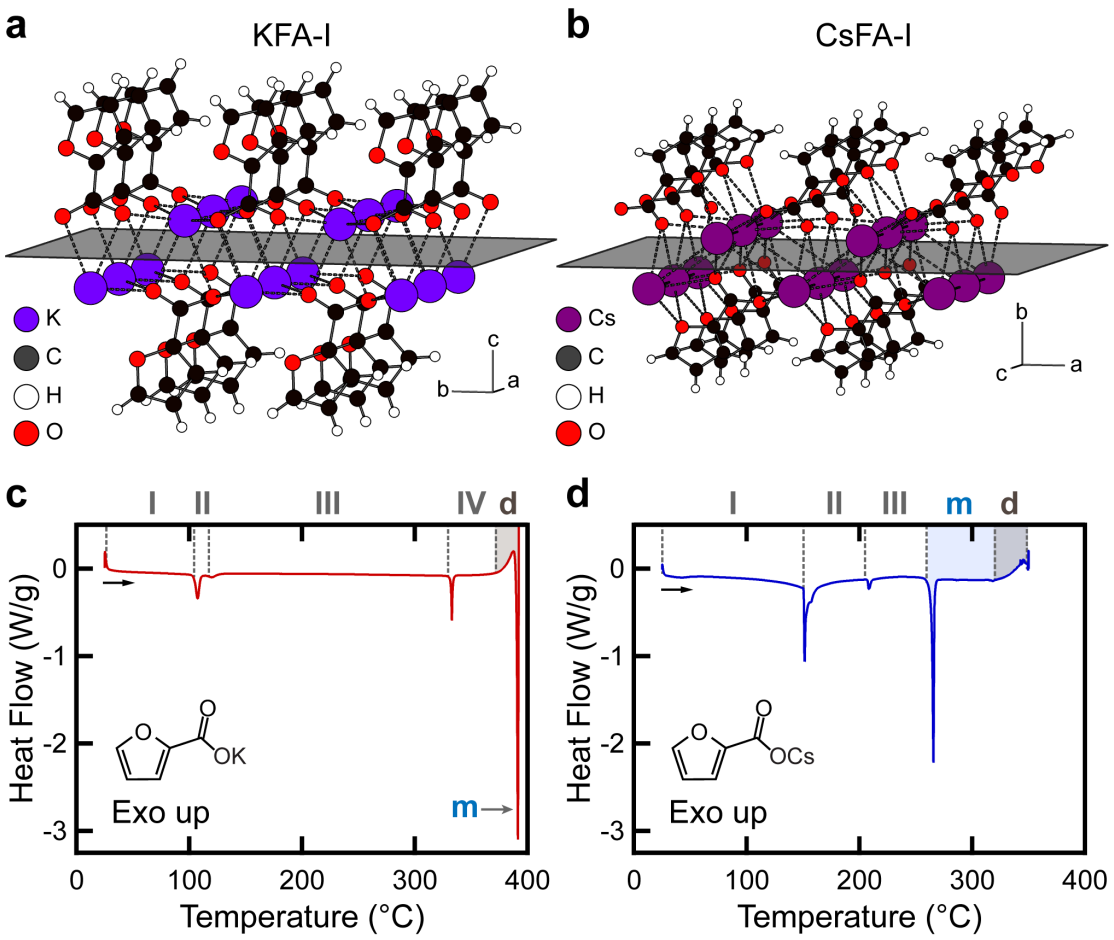

Figure 1 | Structural and thermal properties of alkali furoate salts. **a**, Layered structure of the ambient temperature polymorph of potassium furoate (KFA), as determined from refined single crystal X-ray diffraction data. The (001)-family plane bisecting the cation layer is shown for clarity. **b**, Layered structure of the ambient temperature polymorph of cesium furoate (CsFA), as determined from synchrotron powder X-ray diffraction data by simulated annealing. The (010)-family plane bisecting the cation layer is shown for clarity. **c**,**d**, Differential Scanning Calorimetry heating curves of KFA (**c**) and CsFA (**d**) salts. Temperature regions corresponding to different crystalline polymorphs are labeled above the plots. The region marked "d" corresponds to thermal decomposition, while the peak (or region) marked "m" corresponds to the isotropic melt.

transition for KFA overlaps with its region of thermal decomposition, melting of CsFA occurs approximately 65 °C below the onset of its own decomposition event (T_d = 328 °C). The ability of CsFA to exist in a molten form is crucial for its ability to participate in solvent-free chemistry.

The furoate salt is only one component of the carboxylation reaction medium, however. The stoichiometry of furoate carboxylation promoted by M_2CO_3 requires a minimum of 0.5 molar equivalents of M_2CO_3 relative to MFA in order to achieve complete conversion to the alkali dicarboxylate salt (M_2FDCA). In order to understand the physical properties of the reaction

mixture at the outset of a solvent-free furoate carboxylation reaction, the impact of the addition of M_2CO_3 on the thermal properties of the MFA salt must be examined.

A combination of thermal analysis and variable temperature PXRD reveals that CsFA and Cs_2CO_3 constitute a binary eutectic system (**Fig. 2a**). DSC thermograms were collected for a series of mixtures of CsFA and Cs_2CO_3 salts with varying composition. Increasing the Cs_2CO_3 mole fraction (x) in the mixture affects the position and appearance of the final endothermic transition observed in the DSC heating curve (**Fig. 2b**). When a very small amount of Cs_2CO_3 is present (x = 0.01), the transition shifts to a lower temperature relative to the melting transition observed for pure CsFA. The peak also presents with a distinct shoulder, with the onset of this shoulder occurring at T = 256 °C. For higher values of x, only a single endothermic event is observed, also with an onset temperature of approximately 256 °C. Variable temperature PXRD was used to further examine the nature of this transition, using x = 0.35 to match the 1:0.55 CsFA:Cs_2CO_3 stoichiometry most commonly employed in the synthetic reaction.[10] Comparison of PXRD patterns collected before and after heating this mixture of CsFA and Cs_2CO_3 past 256 °C shows that the transition corresponds to the selective disappearance of diffraction peaks attributable to solid CsFA-III, while anhydrous crystalline Cs_2CO_3 remains (**Fig. 2c**). Moreover, the transition was shown to be reversible. Immediately cooling the mixture upon disappearance of the CsFA peaks leads to their reappearance as CsFA-III recrystallizes at approximately the same temperature (**Fig. 2d**).

These observations are all consistent with a lowering of the CsFA melting point by ~8 °C upon addition of Cs_2CO_3 through formation of a eutectic. For all compositions of relevance to the CsFA carboxylation reaction (i.e. $x \geq 0.33$), the reaction necessarily occurs from a heterogeneous mixture of solid crystalline Cs_2CO_3 and a molten eutectic which contains only a small fraction of the Cs_2CO_3 base. It should be noted that although a two-phase region of coexistence between solid Cs_2CO_3 and molten eutectic is present, the liquidus temperature at which the mixture would theoretically become uniformly molten can never be reached because it lies well beyond the thermal decomposition temperature of CsFA.

In contrast to the CsFA-Cs_2CO_3 system, the analogous mixture with M = K does not exhibit a stable eutectic melt. The absence of eutectic melting was demonstrated using variable temperature

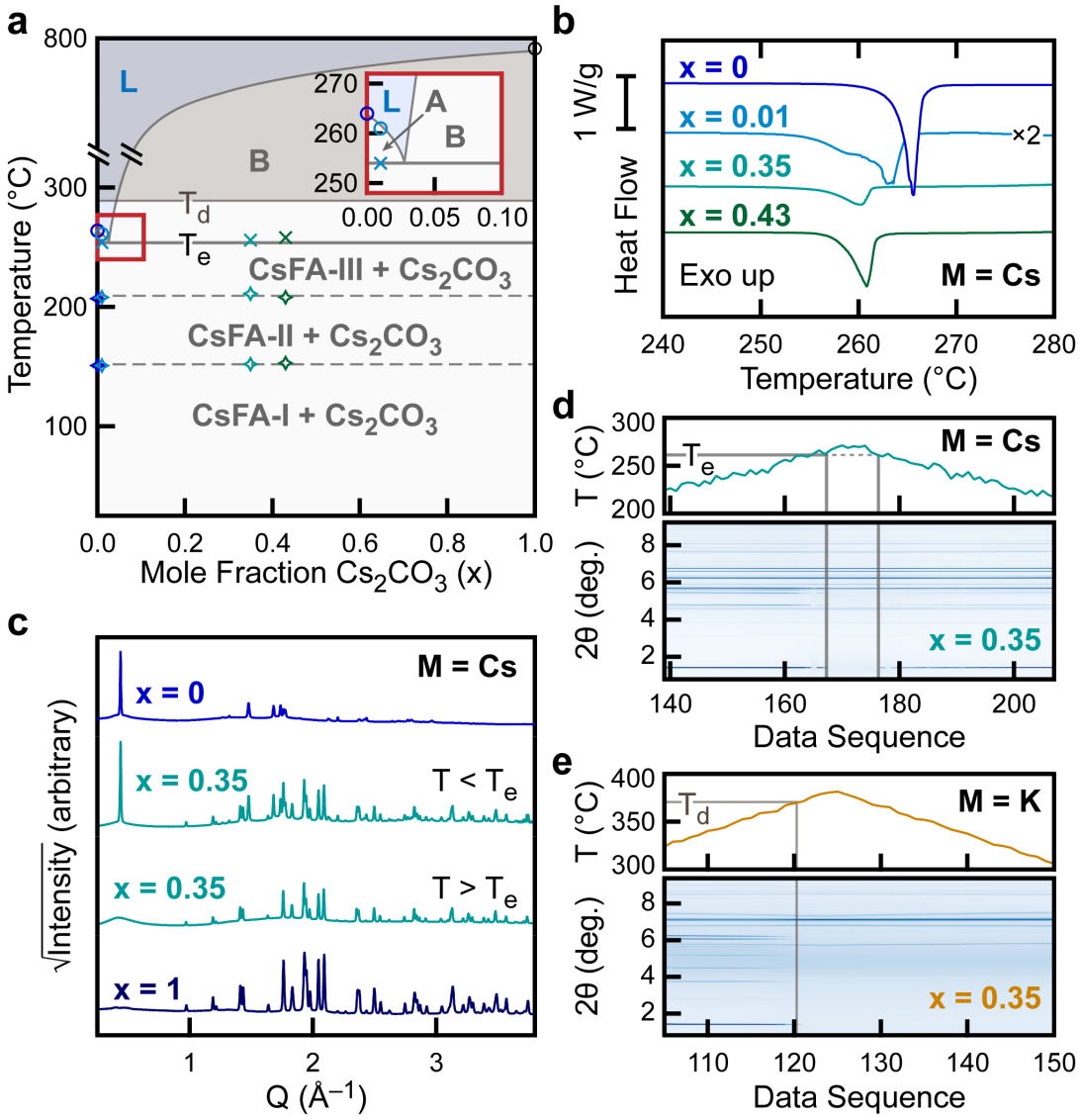

Figure 2 | Phase equilibria in binary MFA-M_2CO_3 mixtures. a, Phase equilibrium diagram for the anhydrous system CsFA-Cs_2CO_3. Marked temperatures of melting transitions (○), eutectic transitions (×), and solid–solid phase transitions (✧) were determined from DSC measurements. All two-phase regions below the eutectic temperature are labeled with their constituent solid phases. The region L corresponds to the uniform melt. The region A (inset) corresponds to the two-phase mixture of CsFA-III + eutectic melt and B corresponds to the two-phase mixture of Cs_2CO_3 + eutectic melt. All regions above the line marked T_d are inaccessible due to decomposition of the CsFA component. **b**, DSC thermograms comparing melting of pure CsFA with eutectic melting in CsFA-Cs_2CO_3 mixtures of varying composition. The trace for x = 0.01 has been scaled vertically to highlight the two distinct thermal events (eutectic formation and liquidus melting) observed. **c**, PXRD patterns comparing a mixture of CsFA and Cs_2CO_3 with x = 0.35 before and after its eutectic melting event. Shown for reference are powder patterns for pure CsFA-III (x = 0) and pure Cs_2CO_3 (x = 1). **d**,**e** Temperature profile (top) and PXRD contour plot (bottom) for variable temperature PXRD (λ = 0.35380, 5 sccm He gas) performed on a mixture of CsFA and Cs_2CO_3 with x = 0.35 (**d**) or KFA and K_2CO_3 with x = 0.35 (**e**). Diffraction intensity in the contour plots increases from white to blue. Melting or decomposition events as evidenced by the disappearance of diffraction peaks are marked.

PXRD. When a mixture of KFA and K_2CO_3 with x = 0.35 was heated, the peaks corresponding to the furoate component eventually disappeared, while the carbonate peaks remained. However, unlike in the cesium-containing mixture, in this case the peaks corresponding to the furoate component did not reappear upon immediate cooling, indicating KFA decomposition rather than a reversible eutectic melting event (**Fig. 2e**). In other words, the addition of K_2CO_3 to KFA does not sufficiently depress the KFA melting point to create a stable two-phase region containing molten KFA below its decomposition temperature.

At elevated temperature and in the presence of CO_2 gas, a mixture of CsFA and Cs_2CO_3 will begin to convert to Cs_2FDCA. If the reaction is performed under flowing conditions, the water produced as a byproduct of carboxylation is stripped away, and the carboxylation process can be envisioned as an interaction between gaseous CO_2 and a three-component mixture of anhydrous salts: CsFA, Cs_2CO_3, and Cs_2FDCA. In an ideal scenario where the reaction proceeds with 100% selectivity to form exclusively Cs_2FDCA, the progression of the reaction from starting material to full conversion can be represented as a traversal through ternary phase space[24, 25] with a compositional constraint dictated by the 2:1 stoichiometric relationship between CsFA and Cs_2CO_3 (**Fig. 3a**). We examined the phase equilibrium of this ternary system by performing thermal and PXRD analysis on samples of CsFA-Cs_2CO_3-Cs_2FDCA mixtures with compositions designed to mimic the progression of a reaction starting from a binary CsFA-Cs_2CO_3 mixture with x = 0.35.

Although Cs_2FDCA by itself is a crystalline solid in the temperature range relevant for CsFA carboxylation (**Figs. S14** and **S15**), conversion of the starting materials to Cs_2FDCA substantially alters the thermal transitions of the mixture compared to the CsFA-Cs_2CO_3 binary phase system. DSC thermograms of anhydrous ternary mixtures prepared to mimic varying extents of conversion in the carboxylation reaction (defined here as Y, $0 \leq Y \leq 1$) show that the accumulation of even small amounts of Cs_2FDCA leads to depression of the system's eutectic temperature T_e below its value in the binary system (**Fig. 3b**). With 25% of the starting CsFA converted to Cs_2FDCA, the mixture's eutectic temperature was lowered to 213 °C, which is ~43 °C below the CsFA-Cs_2CO_3 binary eutectic melting point and within a few degrees of the transition between forms II and III of pure CsFA. Comparison of PXRD patterns taken before and after the eutectic transition in ternary mixtures with Y = 0.05 and 0.25 illustrates which crystalline phases are present in the mixture before and after eutectic melting (**Fig. 3c–e**). This comparison affirms that eutectic melting

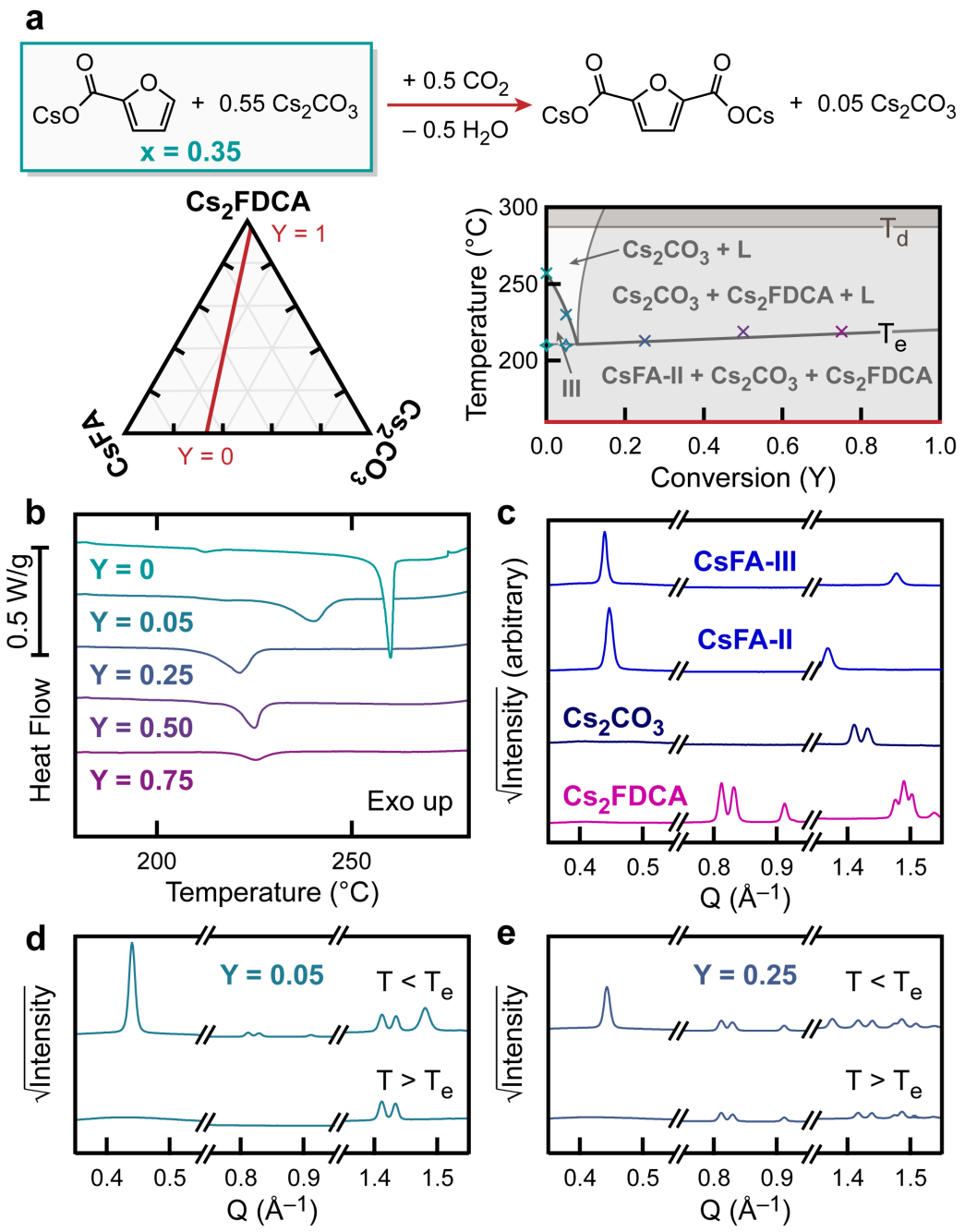

Figure 3 | Phase equilibrium as a function of conversion in a ternary CsFA-Cs_2CO_3-Cs_2FDCA mixture. **a**, Schematic representation of the cesium furoate carboxylation reaction as a cross-section of ternary phase space. Regions in the phase equilibrium diagram (lower right) are labeled with their constituent phases, where "L" corresponds to the molten eutectic phase. The region "III" corresponds to the three-phase region consisting of solid CsFA-III + Cs_2CO_3 + Cs_2FDCA. **b**, DSC thermograms comparing eutectic melting transitions in the ternary mixture as a function of conversion. **c**, Elevated temperature PXRD patterns of individual components of the ternary mixture. Selected regions of the patterns are shown that allow for identification of the constituent crystalline phases in patterns of multi-component mixtures. Patterns shown for Cs_2CO_3 and Cs_2FDCA are for their anhydrous, high temperature forms. **d**,**e**, PXRD patterns comparing ternary mixtures with Y = 0.05 (**d**) and Y = 0.25 (**e**) before and after eutectic melting, demonstrating that Cs_2FDCA is fully dissolved in the melt only at low conversion.

of the CsFA component at higher values of Y occurs directly from CsFA-II, bypassing the CsFA-III polymorph. An additional observation that emerges from this PXRD analysis is that a distinct region exists at low conversions for which the Cs_2FDCA salt is fully soluble in the eutectic melt. Eutectic melting in a mixture with Y = 0.05 presents as the disappearance of diffraction peaks attributable to both the CsFA-III and Cs_2FDCA components (**Fig. 3d**). For a mixture with Y = 0.25, however, Cs_2FDCA diffraction peaks remain even after the disappearance of crystalline CsFA-II (**Fig. 3e**). While increasing conversion leads to lowering of the eutectic melting temperature, the molten eutectic fraction diminishes as the mixture becomes increasingly rich in Cs_2FDCA. This effect can be seen from the decreasing peak area of the endothermic event associated with eutectic melting (**Fig. 3b**). Otherwise put, the carboxylation of CsFA occurs in a mixture that changes its phase composition as a function of conversion. The unique reaction medium is initially a heterogeneous blend of solid and molten material that becomes progressively less molten in character as full conversion is approached.

Finally, we looked to directly observe the carboxylation of CsFA using *operando* PXRD. The results of these studies are consistent with the ternary phase equilibrium model based on the above analysis of ternary mixtures that mimic different extents of conversion, and additionally demonstrate some interesting properties of CsFA as a solvent-free reactant. In two separate experiments, mixtures of CsFA and Cs_2CO_3 with x = 0.35 were heated while flowing CO_2 through the sample capillary at 5 sccm. Following an initial ramp up to the chosen reaction temperature, each sample was held at its setpoint for 70 min while diffraction images were collected continuously. The two chosen setpoints were 260 and 250 °C – above and below the eutectic temperature of the CsFA-Cs_2CO_3 binary mixture, respectively (**Fig. 4a**). As expected, when the reaction was conducted at 260 °C, eutectic melting occurred during the temperature ramp, just prior to reaching 260 °C. As the reaction proceeded and conversion increased, no significant changes were initially observed in the sample's PXRD pattern. However, peaks corresponding to crystalline Cs_2FDCA became visible after approximately 30 min at the reaction temperature had elapsed (**Fig. 4b**). Thus, starting from the binary eutectic melt, carboxylation forms $FDCA^{2-}$ that is initially dissolved in the melt. As conversion increases, a saturation point is reached (somewhere between Y = 0.05 and Y = 0.25) and crystalline Cs_2FDCA forms as an additional phase.

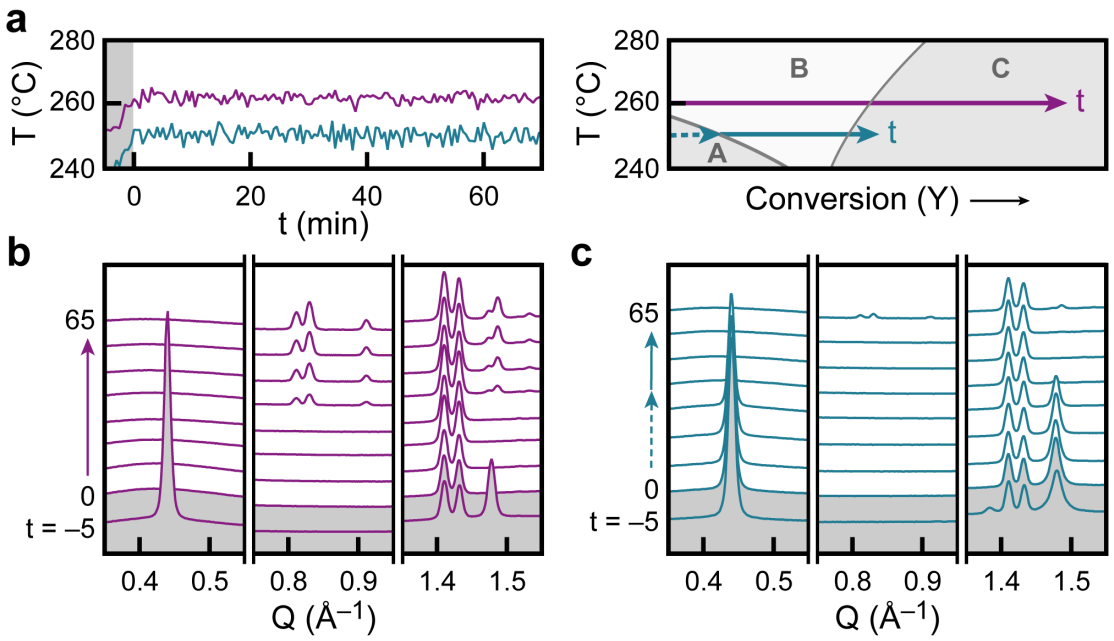

Figure 4 | *Operando* PXRD analysis of cesium furoate carboxylation. **a**, Measured temperature profiles of two *operando* PXRD experiments (left) and representation of ternary phase regions traversed at each temperature (right). Both experiments were performed by heating mixtures of CsFA and Cs_2CO_3 (x = 0.35) while flowing CO_2 gas through the sample capillary at 5 sccm and collecting diffraction images at 30 s intervals. For each experiment, the time $t = 0$ is defined as the point at which the setpoint temperature was first reached. Phase regions in the diagram correspond to CsFA-III + Cs_2CO_3 + Cs_2FDCA (A), Cs_2CO_3 + eutectic melt (B), and Cs_2CO_3 + Cs_2FDCA + eutectic melt (C). **b**,**c**, Selected PXRD patterns showing the evolution of crystalline phases for reactions carried out with setpoint temperatures of 260 °C (**b**) and 250 °C (**c**).

When a fresh sample was heated instead to 250 °C under flowing CO_2, no melting event was initially observed. We anticipated that no Cs_2FDCA formation would occur in the absence of this initial eutectic melting. Surprisingly, after approximately 35 min at 250 °C, spontaneous melting of the CsFA component was observed. As no appreciable change to the sample's temperature occurred during this interval, the occurrence of this melting event must have been induced instead by a change in the mixture composition. At the conclusion of the 70 min reaction period, peaks corresponding to crystalline Cs_2FDCA became barely visible in the PXRD pattern, confirming that carboxylation occurred over the course of the experiment (**Fig. 4c**). This result highlights the melting temperature depression induced by even small amounts of Cs_2FDCA. In addition, it suggests that a small degree of reactivity is possible between CsFA-III and Cs_2CO_3 even without the formation of bulk eutectic domains between the two salts (see **Discussion**). Relative to lower-temperature polymorphs of CsFA and the solid forms of KFA, CsFA-III shows only weak

crystalline ordering (**Figs. S9, S10**), which may be sufficient to enable CsFA to participate in intermolecular reactions.

Integrating the results above, **Figure 5** depicts the evolution of the phase composition for an idealized CsFA carboxylation reaction performed at a temperature just beyond the binary eutectic melting temperature. Upon reaching the eutectic melting temperature, the initial mixture of solid CsFA and Cs_2CO_3 transitions into a mixture of solid and molten components. The molten phase is initially a binary eutectic composed primarily of the low-melting CsFA with a minor amount of Cs_2CO_3; most of the Cs_2CO_3 remains in its solid, crystalline form. As the reaction begins and Cs_2FDCA is formed, it is initially dissolved in the molten phase. With increased conversion, Cs_2FDCA saturates the molten phase and precipitates to form crystalline Cs_2FDCA as an additional solid phase. The reaction proceeds in the ternary eutectic phase with the minor eutectic components (Cs_2CO_3 and Cs_2FDCA) in equilibrium with their corresponding solid phases. Increasing conversion leads to the gradual consumption of the ternary eutectic and solid Cs_2CO_3 components of the mixture as the solid Cs_2FDCA increases.

The idealized reaction presented in **Figure 5** does not account for the small to moderate amounts of decomposition products that are typically observed along with the target Cs_2FDCA product, which complicate the reaction mixture composition.[10, 11] Some of these decomposition products are small-molecule carboxylate salts (e.g. formate, acetate, malonate) that are comparatively low-melting and might alter the phase behavior of the molten component of the reaction mixture. However, the most significant byproduct observed is dense, polymeric char that adds an additional solid component to the heterogeneous mixture. Notwithstanding these additional complexities, the components investigated in the experiments above make up the majority of the material present in the CsFA carboxylation reaction.

The observation of CsFA carboxylation for a reaction performed below the binary eutectic melting temperature (**Fig. 4c**) suggests that it is possible for intermolecular reactions to occur between two solid phases (in this case CsFA-III and Cs_2CO_3). Carboxylation of CsFA initially proceeds in this ostensibly all-solid mixture until formation of a very small amount of the product Cs_2FDCA induces melting as a ternary eutectic. Evidence for intermolecular reactions between species in

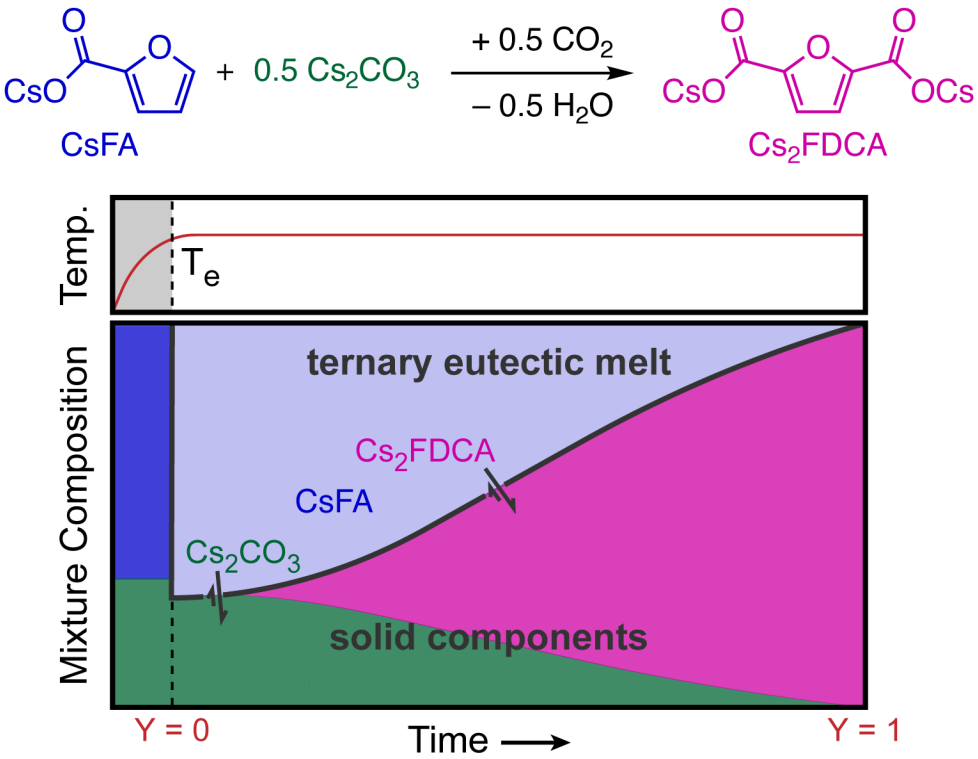

Figure 5 | Evolution of the reaction mixture during solvent-free carboxylation of cesium furoate.

two solid phases has been reported previously,[26-29] although in these cases mechanical energy (e.g. ball milling) was needed to observe reactivity.

The higher melting point of KFA makes it infeasible to perform carboxylation with only KFA and K_2CO_3 because a eutectic cannot be accessed before decomposition. However, we have shown previously that adding a stoichiometric quantity of potassium isobutyrate to the KFA and K_2CO_3 mixture enables carboxylation to occur.[10] Additionally, carboxylation can be performed in high yield using salts composed of furoate and carbonate with a mixture of K^+ and Cs^+ cations, even when only a small proportion of Cs^+ salts is used.[11] While characterizing the phase behavior of these more complicated systems is beyond the scope of this study, the additional degrees of freedom created by using two cations or introducing another anion is expected to give rise to a relatively low-melting eutectic that enables the reaction to proceed.[24, 25] We note that the fraction of the salt mixture that exists in a molten state may be small enough such that there is no visible bulk melting event during a reaction. Regardless of composition, however, furoate carboxylation results in sintering of the salt particles, which is consistent with the formation of molten components during the reaction.

Finally, the results above illuminate the factors that must be addressed in scaling furoate carboxylation. When the carboxylation is performed under quiescent conditions, the evolution of the phase components over time creates mass transport limitations. Specifically, as the ternary eutectic and solid Cs_2CO_3 phases decrease and the solid Cs_2FDCA product accumulates, mass transport of CO_2 and carbonate into the molten phase are expected to become increasingly difficult. Reactor design must therefore take into account the variation in mixture heterogeneity as a function of conversion and maintain a high effective contact area between the molten phase, the CO_2 gas, and the Cs_2CO_3 phase. Reactors that continuously mix or grind the reaction components may be especially useful in this regard.[30, 31]

The combination of PXRD and thermal analysis techniques has provided a detailed description of the phase composition of solvent-free furoate carboxylation. The results demonstrate that the reaction occurs in a molten phase dominated by CsFA with smaller amounts of the Cs_2CO_3 reactant and Cs_2FDCA product. The diminution of the molten component and solid Cs_2CO_3 component as the reaction forms solid Cs_2FDCA presents challenges for maintaining efficient mass transport which need to be managed to achieve optimal yields on large scale. The strategy for analyzing furoate carboxylation described here can be applied to other solvent-free systems to help identify compositional and operational changes that improve performance.

Acknowledgements

This work was supported by the U.S. Department of Energy (DOE) Advanced Research Projects Agency – Energy (ARPA-E) (DE-AR0000961). A.D.F. acknowledges support from a NASA Space Technology Research Fellowship. Powder X-ray diffraction was performed at the Advanced Photon Source, a DOE Office of Science User Facility operated for the DOE Office of Science by Argonne National Laboratory under Contract No. DE-AC02-06CH11357. Thermal analysis was performed at the Stanford Nano Shared Facilities (SNSF), supported by the National Science Foundation under award ECCS-1542152. We thank Jana Maclaren and Andrey Yakovenko for experimental assistance, and Michael Toney and members of the Toney Laboratory for guidance on PXRD structure refinement.

References

1. Loupy, A., Solvent-free Reactions. In *Modern Solvents in Organic Synthesis*, Knochel, P., Ed. Springer Berlin Heidelberg: Berlin, Heidelberg, 1999; pp 153-207.
2. Tanaka, K.; Toda, F., Solvent-Free Organic Synthesis. *Chem. Rev.* **2000,** *100* (3), 1025-1074.
3. Garay, A. L.; Pichon, A.; James, S. L., Solvent-free synthesis of metal complexes. *Chem. Soc. Rev.* **2007,** *36* (6), 846-855.
4. Bala, M. D.; Coville, N. J., Organometallic chemistry in the melt phase. *J. Organomet. Chem.* **2007,** *692* (4), 709-730.
5. Martins, M. A. P.; Frizzo, C. P.; Moreira, D. N.; Buriol, L.; Machado, P., Solvent-free heterocyclic synthesis. *Chem. Rev.* **2009,** *109* (9), 4140-4182.
6. Sarkar, A.; Santra, S.; Kundu, S. K.; Hajra, A.; Zyryanov, G. V.; Chupakhin, O. N.; Charushin, V. N.; Majee, A., A decade update on solvent and catalyst-free neat organic reactions: a step forward towards sustainability. *Green Chem.* **2016,** *18* (16), 4475-4525.
7. Cintas, P.; Tabasso, S.; Veselov, V. V.; Cravotto, G., Alternative reaction conditions: Enabling technologies in solvent-free protocols. *Curr. Opin. Green Sust. Chem.* **2020,** *21*, 44-49.
8. Kulla, H.; Haferkamp, S.; Akhmetova, I.; Röllig, M.; Maierhofer, C.; Rademann, K.; Emmerling, F., In Situ Investigations of Mechanochemical One-Pot Syntheses. *Angew. Chem. Int. Ed.* **2018,** *57* (20), 5930-5933.
9. Julien, P. A.; Germann, L. S.; Titi, H. M.; Etter, M.; Dinnebier, R. E.; Sharma, L.; Baltrusaitis, J.; Friščić, T., In situ monitoring of mechanochemical synthesis of calcium urea phosphate fertilizer cocrystal reveals highly effective water-based autocatalysis. *Chem. Sci.* **2020,** *11* (9), 2350-2355.
10. Banerjee, A.; Dick, G. R.; Yoshino, T.; Kanan, M. W., Carbon dioxide utilization via carbonate-promoted C-H carboxylation. *Nature* **2016,** *531* (7593), 215-9.
11. Dick, G. R.; Frankhouser, A. D.; Banerjee, A.; Kanan, M. W., A Scalable Carboxylation Route to 2,5-Furandicarboxylic Acid. *Green Chem.* **2017,** *19*, 2966-2972.
12. Banerjee, A.; Kanan, M. W., Carbonate-Promoted CO_2 Hydrogenation to Multi-Carbon Oxygenates. *ACS Cent. Sci.* **2018,** *4*, 606-613.
13. Kanan, M. W.; Banerjee, A. Carbonate-promoted carboxylation reactions for the synthesis of valuable organic compounds. U.S. Patent 10,160,740, 2018.
14. Vechorkin, O.; Hirt, N.; Hu, X., Carbon dioxide as the C1 source for direct C-H functionalization of aromatic heterocycles. *Org Lett* **2010,** *12* (15), 3567-9.
15. de Jong, E.; Dam, M.; Sipos, L.; Gruter, G., Furandicarboxylic acid (FDCA), a versatile building block for a very interesting class of polyesters. *Biobased monomers, polymers, and materials* **2012,** *1105*, 1-13.
16. Jensen, M. H.; Riisager, A., Chapter 5 - Advances in the synthesis and application of 2,5-furandicarboxylic acid. In *Biomass, Biofuels, Biochemicals*, Saravanamurugan, S.; Pandey, A.; Li, H.; Riisager, A., Eds. Elsevier: 2020; pp 135-170.
17. Sajid, M.; Zhao, X.; Liu, D., Production of 2, 5-furandicarboxylic acid (FDCA) from 5-hydroxymethylfurfural (HMF): recent progress focusing on the chemical-catalytic routes. *Green Chem.* **2018,** *20* (24), 5427-5453.
18. Lide, D. R., *CRC handbook of chemistry and physics*. CRC press: 2004.
19. Butterhof, C.; Martin, T.; Milius, W.; Breu, J., Microphase separation with small amphiphilic molecules: crystal structure of preservatives sodium benzoate (E211) and potassium benzoate (E212). *Z. Anorg. Allg. Chem.* **2013,** *639* (15), 2816-2821.

20. Coelho, A. A., Whole-profile structure solution from powder diffraction data using simulated annealing. *J. Appl. Crystallogr.* **2000,** *33* (3), 899-908.
21. Hatibarua, J.; Parry, G. S., A crystallographic study of the acetates of potassium, rubidium and caesium. *Acta Crystallogr. B Struct. Sci.* **1972,** *28* (10), 3099-3100.
22. Van Deun, R.; Ramaekers, J.; Nockemann, P.; Van Hecke, K.; Van Meervelt, L.; Binnemans, K., Alkali-Metal Salts of Aromatic Carboxylic Acids: Liquid Crystals without Flexible Chains. *Eur. J. Inorg, Chem.* **2005,** *2005* (3), 563-571.
23. Nelson, P. N.; Taylor, R. A., Theories and experimental investigations of the structural and thermotropic mesomorphic phase behaviors of metal carboxylates. *Appl. Petrochem. Res.* **2014,** *4* (3), 253-285.
24. Rothenberg, G.; Downie, A. P.; Raston, C. L.; Scott, J. L., Understanding solid/solid organic reactions. *J. Am. Chem. Soc.* **2001,** *123* (36), 8701-8708.
25. Daněk, V., Chapter 3 - Phase Equilibria. In *Physico-Chemical Analysis of Molten Electrolytes*, Daněk, V., Ed. Elsevier Science: Amsterdam, 2006; pp 107-219.
26. Braga, D.; Grepioni, F., Reactions between or within molecular crystals. *Angew. Chem. Int. Ed.* **2004,** *43* (31), 4002-4011.
27. Balema, V. P.; Wiench, J. W.; Pruski, M.; Pecharsky, V. K., Mechanically induced solid-state generation of phosphorus ylides and the solvent-free wittig reaction. *J. Am. Chem. Soc.* **2002,** *124* (22), 6244-6245.
28. Balema, V. P.; Wiench, J. W.; Pruski, M.; Pecharsky, V. K., Solvent-free mechanochemical synthesis of two Pt complexes: cis-$(Ph_3P)_2PtCl_2$ and cis-$(Ph_3P)_2PtCO_3$. *Chem. Comm.* **2002,** (15), 1606-1607.
29. Dolotko, O.; Wiench, J. W.; Dennis, K. W.; Pecharsky, V. K.; Balema, V. P., Mechanically induced reactions in organic solids: liquid eutectics or solid-state processes? *New J. Chem.* **2010,** *34* (1), 25-28.
30. Crawford, D. E.; Miskimmin, C. K. G.; Albadarin, A. B.; Walker, G.; James, S. L., Organic synthesis by Twin Screw Extrusion (TSE): continuous, scalable and solvent-free. *Green Chem.* **2017,** *19* (6), 1507-1518.
31. Rodriguez, B.; Bruckmann, A.; Rantanen, T.; Bolm, C., Solvent-free carbon-carbon bond formations in ball mills. *Adv. Synth. Catal.* **2007,** *349* (14-15), 2213-2233.

Supporting Information

Phase Behavior that Enables Solvent-Free Carbonate-Promoted Furoate Carboxylation

Amy D. Frankhouser and Matthew W. Kanan*

Department of Chemistry, Stanford University, Stanford, California 94305, United States

Table of Contents **Page**

1. Methods

1.1 Materials

Anhydrous potassium carbonate (99.8%) was purchased from Fisher Chemical, cesium carbonate (99.9%) was purchased from Chem Impex International, and 2-furoic acid (98%) was purchased from Acros Organics. Furan-2,5-dicarboxylic acid was synthesized and isolated according to a previously reported procedure,[1] and its purity was verified by ^{1}H and ^{13}C NMR prior to use. Anhydrous diethyl ether (99%) and methanol (99.9%) were purchased from Fisher Chemical and used without further purification. D_2O (99.9%) and deuterated dimethyl sulfoxide (d6, 99.9%) were purchased from Cambridge Isotope Laboratories. Sodium L-(+)-tartrate dihydrate (99.4%) was purchased from Fisher Chemical. CO_2 (99.5%) was purchased from Praxair.

1.2 Preparation of alkali carboxylate salts and salt mixtures

Standardized 1.75 M solutions of cesium carbonate (Cs_2CO_3) and potassium carbonate (K_2CO_3) were prepared by dissolving massed quantities of the anhydrous carbonates in an appropriate volume of deionized water. These solutions were used to prepare the carboxylate salts of 2-furoic acid (FA) and furan-2,5-dicarboxylic acid (FDCA) by adding 0.5 molar equivalents (for FA) or 1.0 molar equivalents (for FDCA) of M_2CO_3 stock solution to a massed quantity of the anhydrous (di)carboxylic acid. After allowing the acid and carbonate base to fully react, the resulting carboxylate salt solutions were diluted with deionized water and stored as 0.5 M solutions. Concentration of the organic anion in each solution was verified by ^1H NMR in D_2O with sodium L-(+)-tartrate dihydrate salt used as an integration standard.

Individual carboxylate salts were prepared as solid powders by evaporating a quantity of standard solution to dryness in a heated aluminum vial block thermostatted at 150 °C. Mixtures of carboxylate and carbonate salts were prepared by mixing appropriate volumes of standard solutions to achieve the desired molar ratio, then drying the mixture in the same manner. The mixed powders were then thoroughly ground with a spatula to ensure sample homogeneity.

It should be noted that cesium salts are hygroscopic to varying degrees, which can complicate sample preparation and handling unless measures are taken to rigorously exclude moisture. Additionally, when solid cesium furoate (CsFA) is exposed to atmosphere in the presence of even small amounts of excess carbonate base, it will take on atmospheric moisture and begin to degrade from the presence of concentrated trace hydroxide, evidenced by increasing brown discoloration of the solid over time (hours–days). To address this, efforts were made to prepare fresh samples of any CsFA-containing solids shortly before their use in characterization experiments. When this was impossible, the samples were stored under moisture-free conditions (N_2 or Ar atmosphere).

1.3 Thermal Analysis

Differential Scanning Calorimetry (DSC) was performed on a TA Instruments Q2000 Differential Scanning Calorimeter. Samples of individual or mixed salts ranging in total mass from 1–10 mg were sealed in standard aluminum "Tzero" pans with lids, purchased from TA Instruments. Heat flow to the sample in mW was recorded relative to a reference pan and lid prepared without sample. Unless otherwise noted, measurements were performed under 50 mL/min dry N_2 flow with a temperature ramp rate of 5 °C/min. Onset temperatures for phase transitions and other thermal events were determined using TA Instruments Universal Analysis software.

As salt samples could not be kept rigorously moisture-free during the preparation of DSC sample pans, the amount of adventitious moisture and/or degree of hydration present in the sample prior to the start of the DSC protocol is unknown. Heat flows are thus reported in units of W/g, where the mass of sample has been uncorrected to account for the presence of water.

Thermogravimetric analysis (TGA) was performed on a TA Instruments SDT650 Simultaneous Thermal Analyzer. Samples of individual salts ranging in total mass from 5–20 mg were placed in tared ceramic sample pans purchased from TA Instruments, and changes in sample mass were recorded while applying a temperature ramp. Unless otherwise noted, measurements were performed under 50 mL/min dry N_2 flow with a temperature ramp rate of 5 °C/min.

Polarized Optical Microscopy was performed using a Nikon LV100 microscope equipped with an Instec heating stage. Anhydrous salt samples were prepared for microscopy by placing a drop of an aqueous solution of the desired salt or salt mixture on a standard glass slide, applying a cover slip, then drying on a hotplate surface at ~180 °C. For samples containing cesium salts, slides were transported to the microscope under N_2 atmosphere and quickly transferred to the heating stage, which was preheated to at least 100 °C, in order to prevent moisture accumulation. Samples were imaged at 10× magnification through crossed polarizers. Sample temperature was modified by adjusting the heating stage setpoint, typically with a ramp rate of 10 °C/min. Phase transitions were visually identified by significant changes in sample morphology (solid-solid transitions) or by the loss of birefringence (melting), and the approximate onset temperature of any observable transition was noted.

1.4 Single crystal X-ray diffraction of potassium furoate

Experimental details

Potassium furoate (KFA) was crystallized by vapor diffusion of diethyl ether into a solution of KFA in methanol at ambient temperature, yielding small, colorless needles. A single crystal of KFA with approximate dimensions of 60×85×450 μm was transferred to a Kapton loop and mounted in a Bruker D8 Venture diffractometer equipped with a Photon100 area detector and an Oxford Cryosystems cryostream. The crystal was cooled to 100 K for data collection, and frames were collected with Mo Kα radiation (λ = 0.71073 Å) while performing ω and φ scans. The data were used for refinement of the unit cell, then integrated and reduced using SAINT v8.37a and corrected for absorption effects using SADABS v2016/2.[2] Space group determination and structure solution were performed using SHELXT, and refinement was performed by full-matrix least squares analysis of F^2 using SHELXL v2014/7 as implemented in Olex2 software.[3–5] The structure was refined as a two-component inversion twin. Hydrogen atoms were added in calculated positions, and all non-H atoms were refined anisotropically.

Crystallographic data

Formula	$C_5H_3KO_3$	
Formula weight	150.17	
Temperature	100 K	
Crystal system	Orthorhombic	
Space group	$P2_12_12_1$	
Unit cell dimensions	a = 3.9649(2) Å	α = 90°
	b = 5.7919(4) Å	β = 90°
	c = 25.7992(16) Å	$\gamma = 90°$
Volume	592.46(6) Å^3	
Z	4	
R_1, wR_2 ($I < 2(\sigma)$)	R_1 = 0.0290, wR_2 = 0.0552	
R_1, wR_2 (all data)	R_1 = 0.0355, wR_2 = 0.0572	
GoF	1.079	

1.5 Powder X-ray diffraction measurements

High resolution powder diffraction

High-resolution synchrotron powder X-ray diffraction data were collected at Beamline 11-BM at the Advanced Photon Source (APS). All samples were prepared by drying under flowing N_2 (1 h, 150 °C) and vacuum (3 h) to remove residual water before transferring to a N_2-atmosphere glovebox. Inside the glovebox, samples were finely ground and packed into 0.5 mm O.D. borosilicate capillaries. Capillaries were sealed temporarily using a plug valve (Swagelok) adapted to a 1/8" Ultratorr fitting, removed from the glovebox, then flame sealed under vacuum. Diffraction patterns were collected at ambient temperature with a wavelength of 0.412723 Å. Diffraction data were collected using discrete detectors covering an angular range from –6° to 16º 2θ. The detectors were scanned over a 34º 2θ range, with data points collected every 0.001º 2θ at a scan speed of 0.01º s^{-1}. Corrections were applied for detector sensitivity, 2θ offset, small differences in wavelength between detectors, and the source intensity, before merging the data into a single set of intensities evenly spaced in 2θ.

Variable temperature and in situ *powder diffraction*

Variable temperature and controlled atmosphere powder X-ray diffraction datasets were collected at Beamline 17-BM at the APS. Samples to be measured under air-free conditions were prepared in vacuum-sealed 0.7 mm O.D. borosilicate capillaries using the procedure described above. Samples to be measured under controlled atmosphere conditions were prepared as loose powders, shipped under N_2 atmosphere, and packed into Kapton capillaries inside of an Ar-atmosphere glove bag immediately prior to measurement. Both capillary-sealed and loose powder samples were loaded into 1.2 mm O.D. Kapton or quartz capillaries and secured between glass wool plugs. The capillaries were installed in a flow cell/furnace assembly, described in detail elsewhere.[6] Diffraction images were collected at a wavelength of 0.35488 Å, 0.34753 Å, or 0.35380 Å and recorded on a flat panel amorphous silicon area detector (PerkinElmer PE1621 or VAREX XRD4343CT).

Images were collected continuously while flowing either He or CO_2 gas at 5 sccm through the capillary and heating the sample to a setpoint temperature controlled by a K-type thermocouple (Omega KMQIN-010U-6) inserted into the heated portion of the sample capillary. Some variability in the recorded temperatures of phase transitions and other thermal events was noted between experiments, likely related to slight variability in the placement of the thermocouple and/or the density of packing within the sample capillary; however, the number, order, and relative spacing between thermal events was consistent in all cases between PXRD experiments and with corresponding thermal analysis data. Unless otherwise mentioned, a temperature ramp rate of 3 °C min^{-1} was used for sample heating and cooling. Each image was collected with a total exposure time of 30 s (cesium-containing samples) or 60 s (potassium-containing samples) while rocking the sample capillary through a 15° angle. The resulting 2D diffraction images were integrated to convert to intensity vs. 2θ using GSAS-II software.

1.6 Furoate structure refinement and solution

Rietveld refinement of potassium furoate form I structure

Structure refinement of the single crystal potassium furoate (KFA) structure obtained under cryogenic conditions (100 K) was performed using a high-resolution powder X-ray diffraction pattern collected for KFA at ambient temperature. Using TOPAS Academic software,[7] unit cell parameters for the powder pattern were first estimated using a standard peak search followed by indexing.[8] The resulting space group and approximate unit cell dimensions showed excellent agreement with those of the single crystal structure, with the exception of a slightly lengthened *c* lattice parameter (~0.5 Å difference) for the ambient temperature pattern. Following a structureless Pawley refinement to determine an initial estimate for background and peak profile parameters, Rietveld refinement was performed using the KFA single crystal structure as the structural model. A preferred orientation term was introduced using the March-Dollase model.[9] Satisfactory agreement between the experimental and predicted patterns (R_{wp} = 9.7%, χ^2 = 1.28) was obtained by refinement of background, peak profile, preferred orientation, and lattice parameters, and the fractional coordinates of the potassium atom site.

Structure solution for cesium furoate form I by simulated annealing

A plausible structure for the anhydrous room temperature polymorph of cesium furoate (CsFA-I) was determined using ambient temperature powder X-ray diffraction patterns collected independently at two different beamlines for anhydrous samples of CsFA. Both patterns were indexed after performing a standard peak search in TOPAS Academic. Cross-referencing of indexing solutions for the two patterns was used to determine a space group assignment of $P2_1$ and an initial estimate of unit cell dimensions. The unit cell, background, and peak profile parameters were initially refined in a structureless Pawley refinement of the high-resolution pattern (λ = 0.412723 Å) and fixed during the subsequent simulated annealing procedure.

A structural model was created by defining sites for two symmetry-independent CsFA ($CsC_5H_3O_3$) units. The furoate anion was described as a rigid body using atomic coordinates determined from the single crystal structure of KFA, while the cesium cations were refined as independent sites. All atoms and rigid bodies were initialized to arbitrary positions within the unit cell, and simulated annealing was carried out by refining the atomic coordinates of the cesium sites along with translation and rotation terms for the furoate anions.[10] The resulting *ab initio* structure for CsFA showed considerable similarities with the refined KFA structure as well as reasonable Cs–O bond distances in the coordinating carboxylate groups,[11] and was therefore accepted for further refinement.

A final cycle of Rietveld refinement was applied to the resulting structure against each of the two PXRD patterns that were initially used for indexing. Refined parameters included background and peak profile terms, lattice parameters, fractional coordinates of the cation sites, and translation/rotation terms for the anion rigid bodies. In each case, the refinement resulted in reasonable visual agreement between the simulated and experimental patterns (R_{wp} values of 16.6% and 9.6%, χ^2 values of 3.98 and 8.22, respectively), and the layered packing geometry of the structural model was retained.

2. Supplementary Figures

a

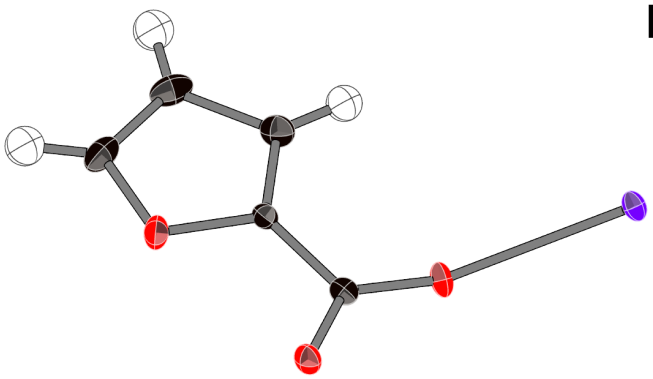

b

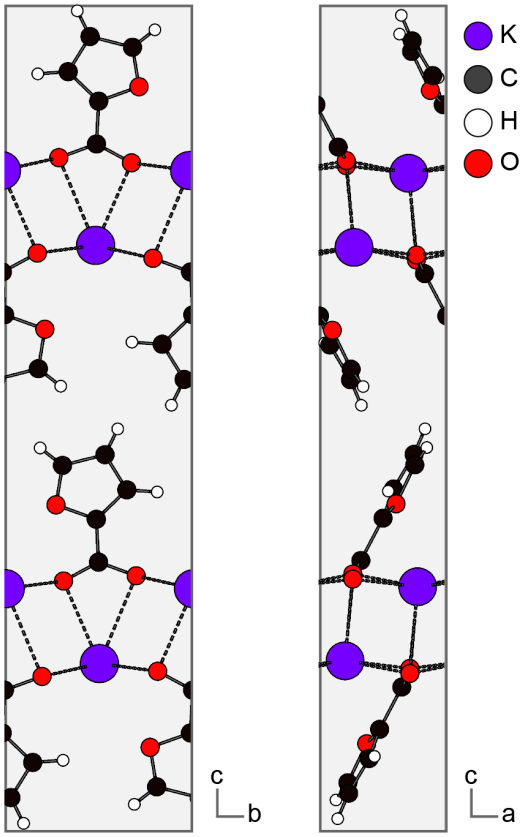

c

Potassium 2-furoate ($KC_5H_3O_3$)	
temperature	100 K
space group	$P\,2_12_12_1$
a × b × c	4.0 × 5.8 × 25.8 Å
Z	4

Figure S1 | X-ray crystal structure of potassium furoate. **a**, Asymmetric unit of the structure containing a single potassium furoate ($KC_5H_3O_3$) unit. Non-H atoms are rendered as 50% thermal ellipsoids. **b**, Views of the unit cell along its *a* and *b* axes, illustrating layered packing. **c**, Selected measurement and unit cell parameters for the single crystal structure.

a

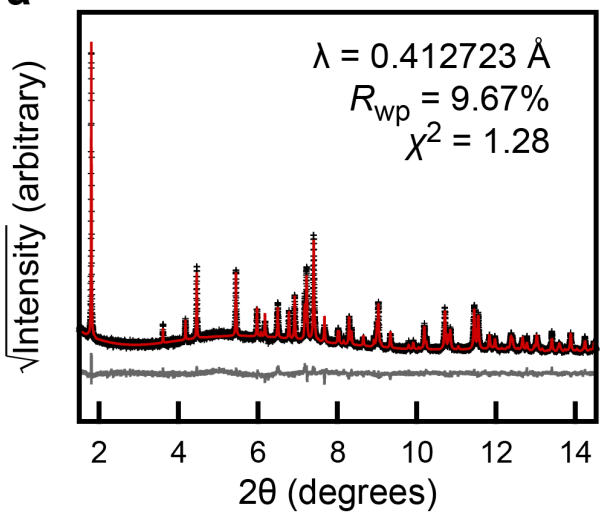

b

Potassium 2-furoate ($KC_5H_3O_3$)	
temperature	25 °C
space group	$P\,2_12_12_1$
a × b × c	4.0 × 5.8 × 26.2 Å

Figure S2 | Rietveld refinement of potassium furoate single crystal structure. **a**, Measured (black), simulated (red), and difference (gray) diffraction patterns for anhydrous potassium furoate at ambient temperature, following refinement of the single crystal structure. **b**, Selected measurement and refined unit cell parameters.

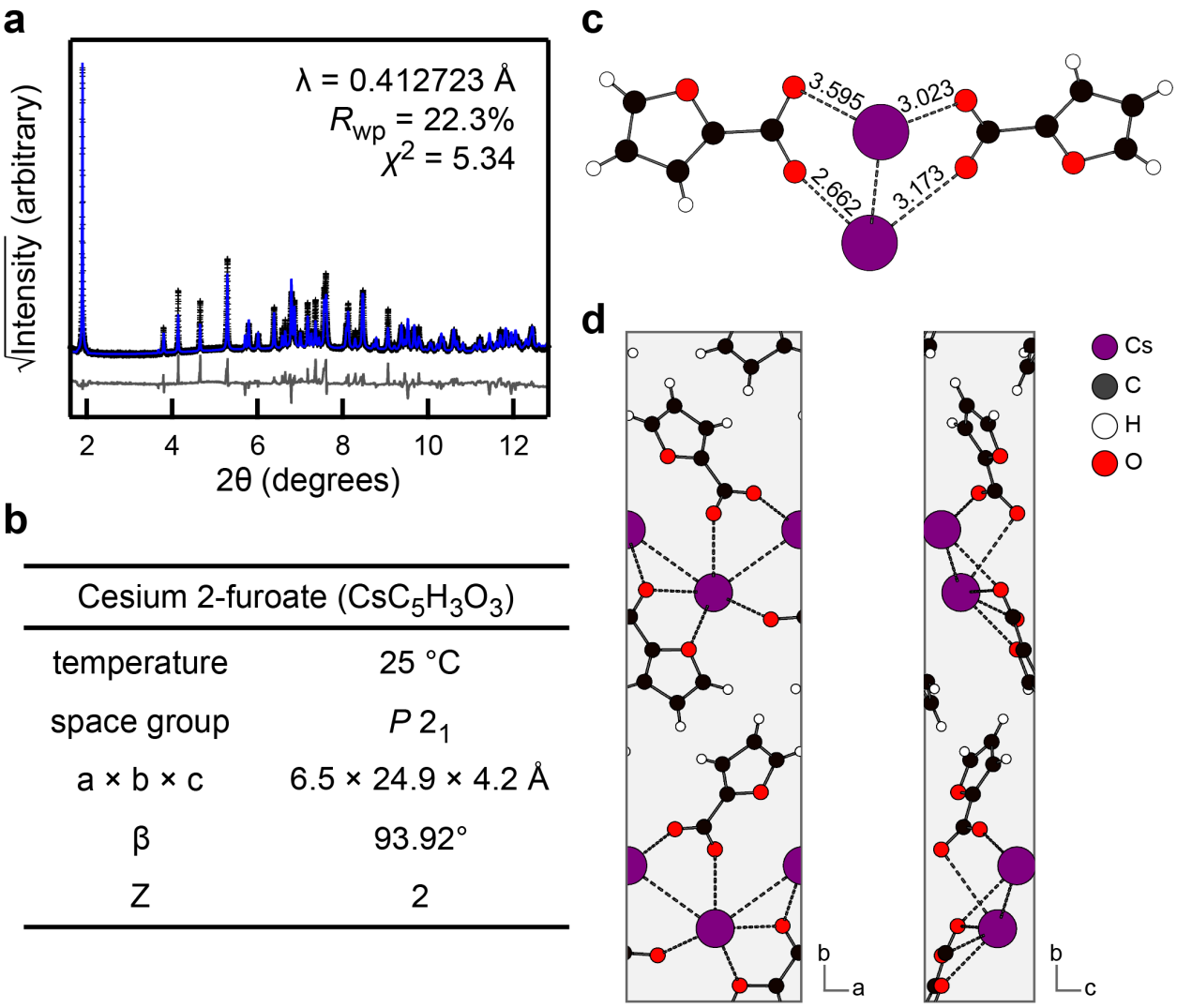

b

Cesium 2-furoate ($CsC_5H_3O_3$)	
temperature	25 °C
space group	$P\,2_1$
a × b × c	6.5 × 24.9 × 4.2 Å
β	93.92°
Z	2

Figure S3 | Ambient temperature structure of anhydrous cesium furoate. **a**, Measured (black), simulated (blue), and difference (gray) diffraction patterns for the best-fit structure determined by simulated annealing prior to additional refinement. The measured PXRD pattern was collected using an anhydrous sample of CsFA at ambient temperature. **b**, Selected measurement and unit cell parameters for the resulting structure. **c**, Asymmetric unit of the structure containing two symmetry-independent cesium furoate ($CsC_5H_3O_3$) units. Bond distances (in Å) between carboxylate group oxygen atoms and cesium cations are shown. All atoms were defined as thermally isotropic sites and are rendered as spheres. **d**, Views of the unit cell along its *c* and *a* axes, illustrating layered packing.

a

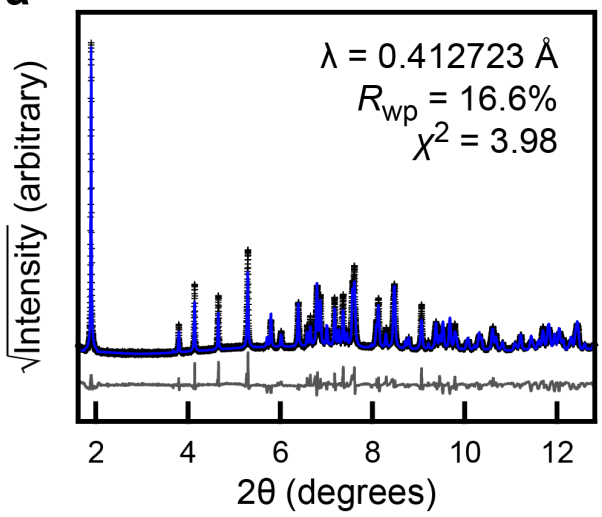

b

Cesium 2-furoate ($CsC_5H_3O_3$)	
temperature	25 °C
space group	$P\,2_1$
a × b × c	6.5 × 24.9 × 4.2 Å
β	93.92°

Figure S4 | Refinement of simulated CsFA-I structure. **a**, Refinement against high resolution synchrotron powder X-ray diffraction pattern of anhydrous CsFA collected at ambient temperature. Shown are the measured (black), simulated (blue), and difference (gray) patterns. **b**, Selected measurement and refined unit cell parameters.

a

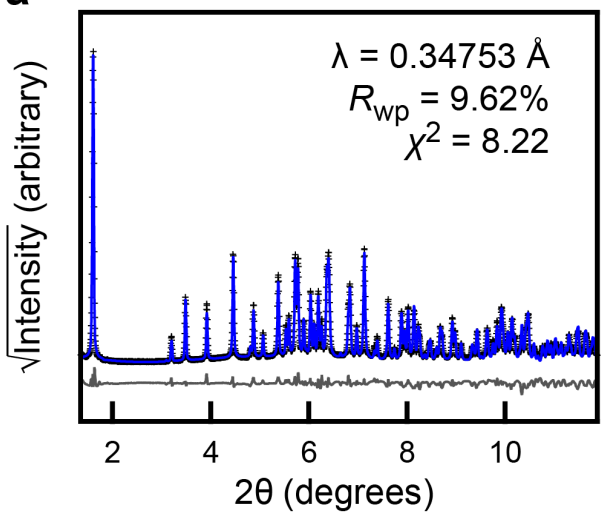

b

Cesium 2-furoate ($CsC_5H_3O_3$)	
temperature	23 °C
space group	$P\,2_1$
a × b × c	6.5 × 24.8 × 4.2 Å
β	93.96°

Figure S5 | Refinement of simulated CsFA-I structure. **a**, Refinement against synchrotron powder X-ray diffraction pattern of CsFA collected at ambient temperature under 5 sccm flow of He gas. Shown are the measured (black), simulated (blue), and difference (gray) patterns. **b**, Selected measurement and refined unit cell parameters.

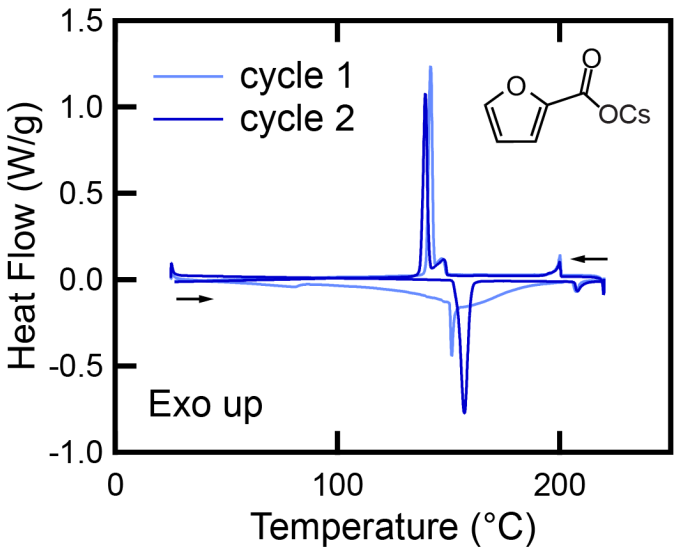

Figure S6 | Differential Scanning Calorimetry of cesium furoate with multiple heating/cooling cycles. Cesium furoate (CsFA) takes on adventitious moisture during preparation of the DSC sample pan, which is lost during the first heating cycle. The endothermic event assigned to the transition CsFA-I → CsFA-II remains on the second cycle, confirming that the sharp transition at at T ~ 150 °C corresponds to a phase transition between two anhydrous crystalline phases rather than a dehydration event. Note that the effects of adventitious moisture are entirely absent by the temperature at which the CsFA-II → CsFA-III transition occurs.

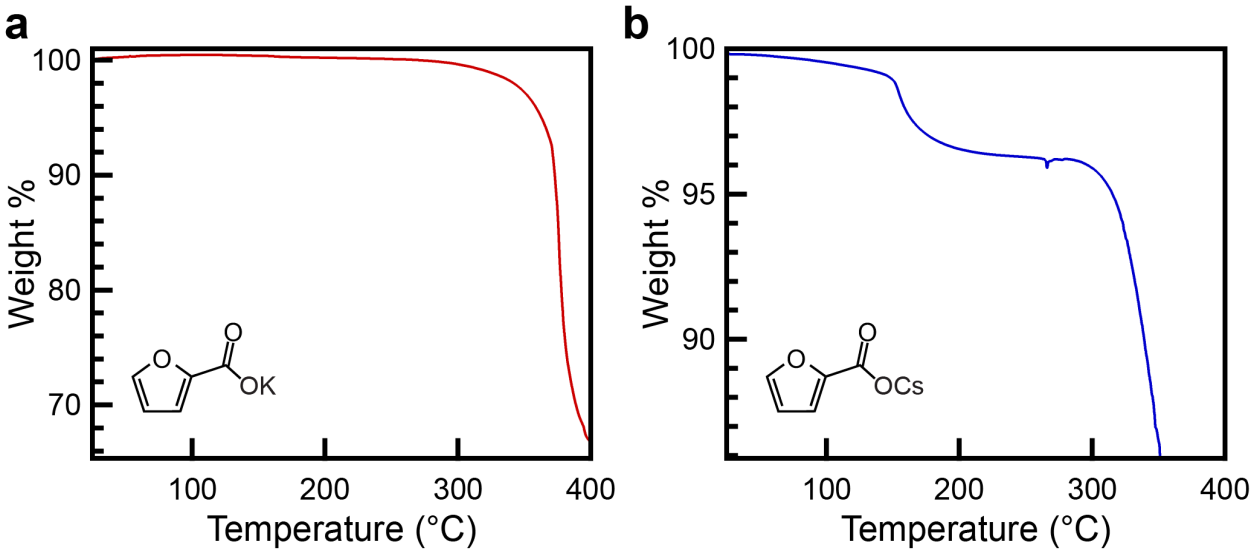

Figure S7 | Thermogravimetric analysis of potassium and cesium furoate salts. **a**, TGA curve of potassium furoate (KFA), showing a single mass loss event at ~390 °C attributed to decomposition. **b**, TGA curve of cesium furoate (CsFA), showing two mass loss events occurring at ~150 °C and ~300 °C. The first event is attributed to loss of adventitious moisture that accumulated during preparation of the sample, while the second is consistent with thermal decomposition.

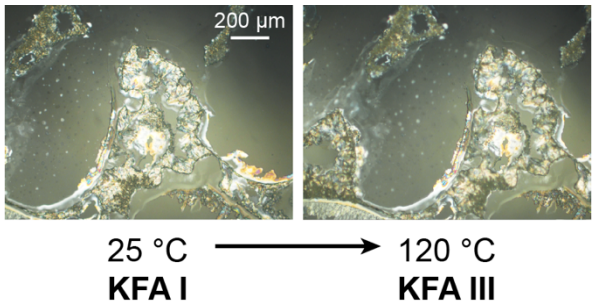

Figure S8 | Polarizing Optical Microscopy of potassium furoate. A 10× magnified image of potassium furoate (KFA) is shown before and after heating through the solid-solid phase transitions KFA-I → KFA-II and KFA-II → KFA-III. The salt remains in a crystalline state, and no significant changes in texture or morphology are observed. The transitions KFA-III → KFA-IV and the melting/decomposition event could not be observed due to the temperature limit of the microscope hot stage.

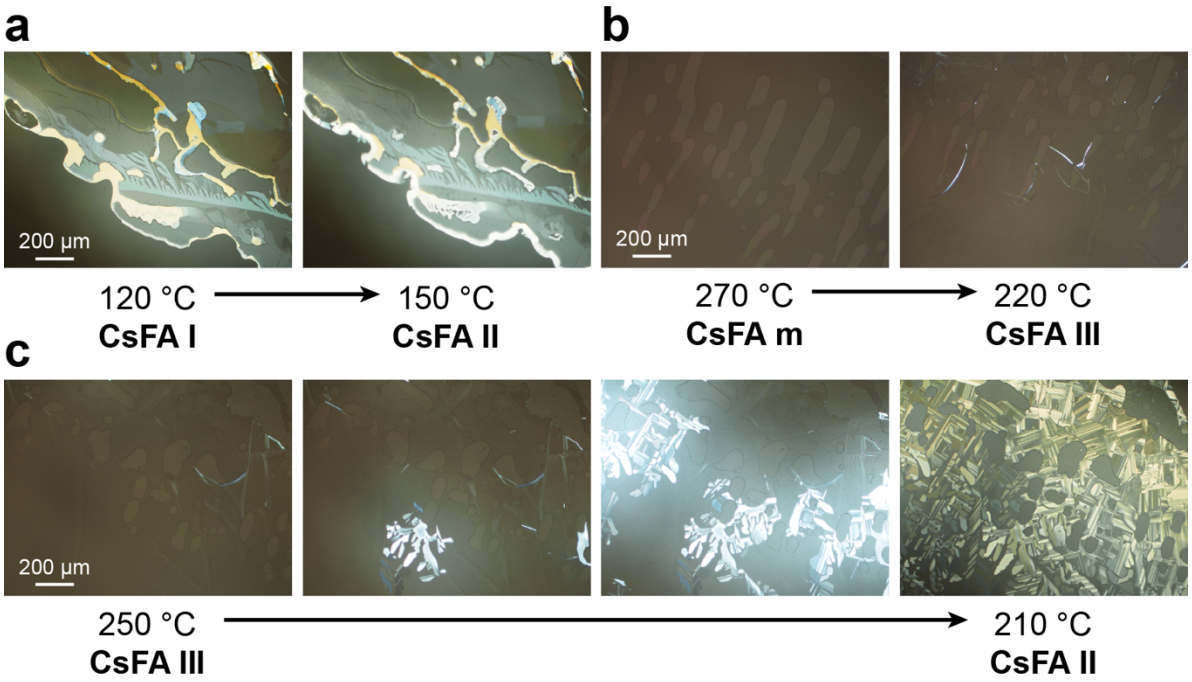

Figure S9 | Polarizing Optical Microscopy of cesium furoate. **a**, Images before and after heating through the solid-solid phase transition CsFA-I → CsFA-II. The sample after drop-drying exhibits a mosaic-like texture, and the transition is apparent from subtle changes along the edges between crystalline domains. **b**, Images before and after cooling from the isotropic melt. The CsFA-III phase appears from the molten liquid as weakly birefringent streaks. **c**, Successive images that show cooling through the phase transition CsFA-III → CsFA-II. The CsFA-II polymorph has a striped texture with much stronger birefringence than CsFA-III.

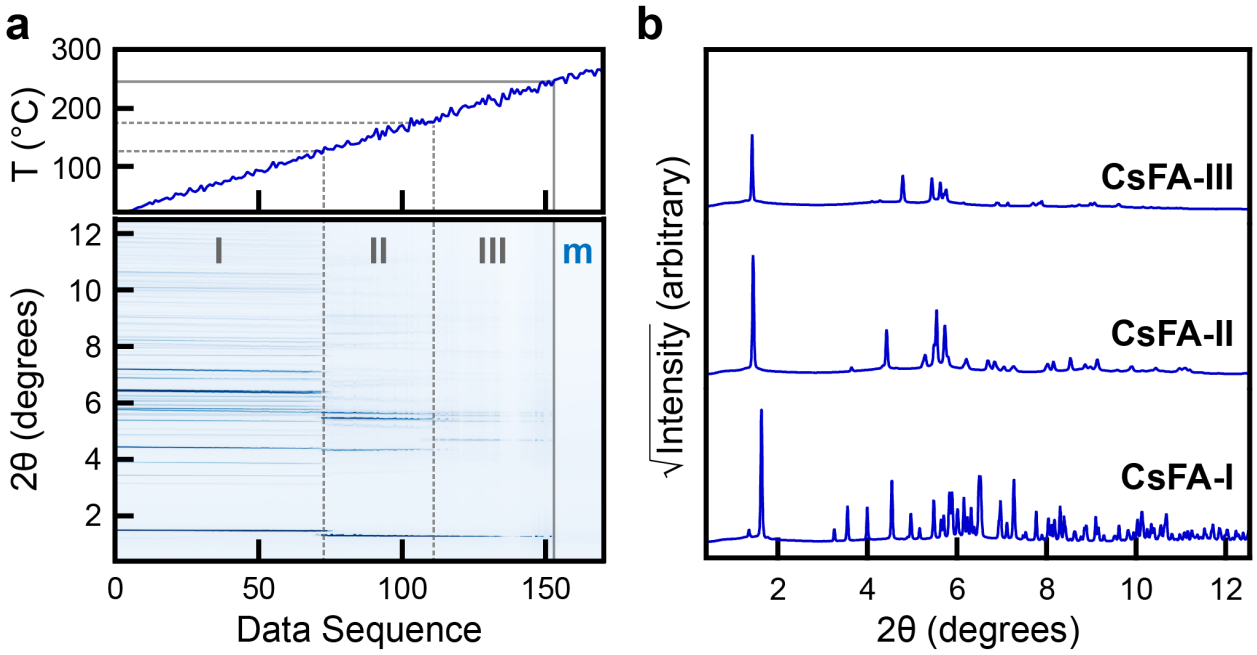

Figure S10 | Variable temperature PXRD of anhydrous cesium furoate. **a**, Temperature profile (top) and contour plot (bottom) of successive PXRD measurements collected while heating a sample of cesium furoate (CsFA) sealed under vacuum in a borosilicate capillary. Diffraction images were collected with $\lambda = 0.35488$ Å every 30 s while heating with a setpoint ramp rate of 3 °C min^{-1}. Diffraction intensity in the contour plot increases from white to blue. Solid–solid and melting transitions are visible as the shifting and disappearance of diffraction peaks, respectively. **b**, Individual PXRD patterns for the three crystalline polymorphs of anhydrous CsFA selected from the corresponding regions of the contour plot.

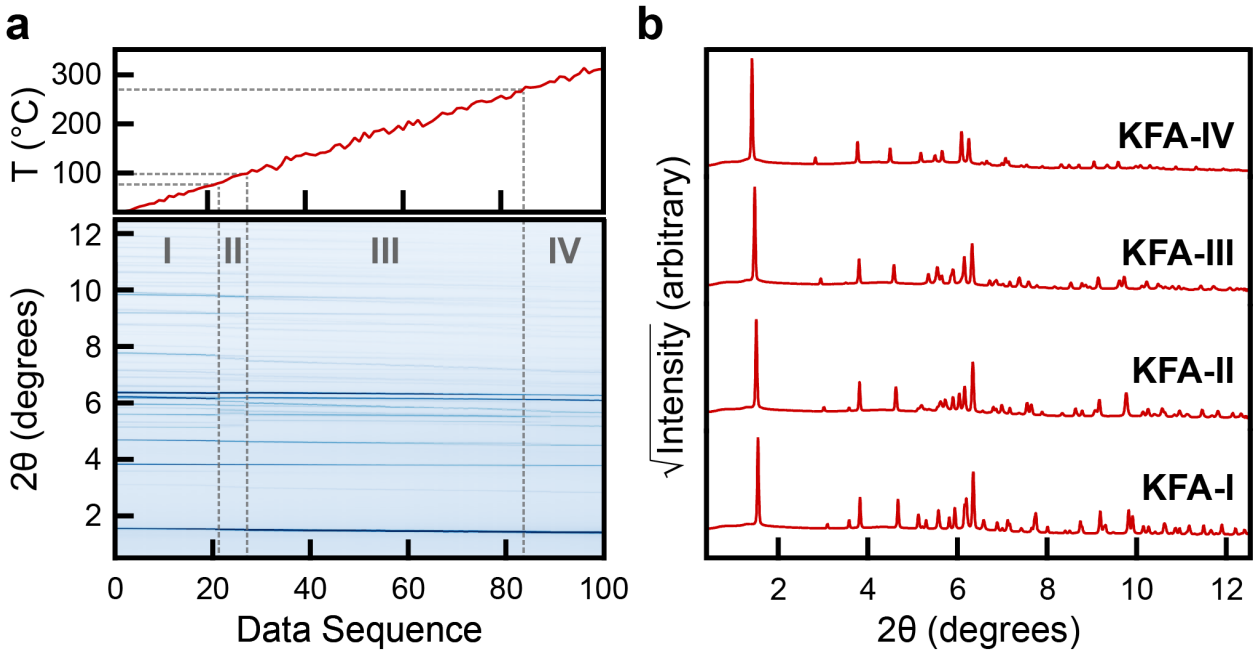

Figure S11 | Variable temperature PXRD of anhydrous potassium furoate. **a**, Temperature profile (top) and contour plot (bottom) of successive PXRD measurements collected while heating a sample of potassium furoate (KFA) sealed under vacuum in a borosilicate capillary. Diffraction images were collected with $\lambda = 0.35488$ Å every 60 s while heating with a setpoint ramp rate of 3 °C min^{-1}. Diffraction intensity in the contour plot increases from white to blue. Solid–solid transitions are visible as the shifting of diffraction peaks. **b**, Individual PXRD patterns for the four crystalline polymorphs of anhydrous CsFA selected from the corresponding regions of the contour plot.

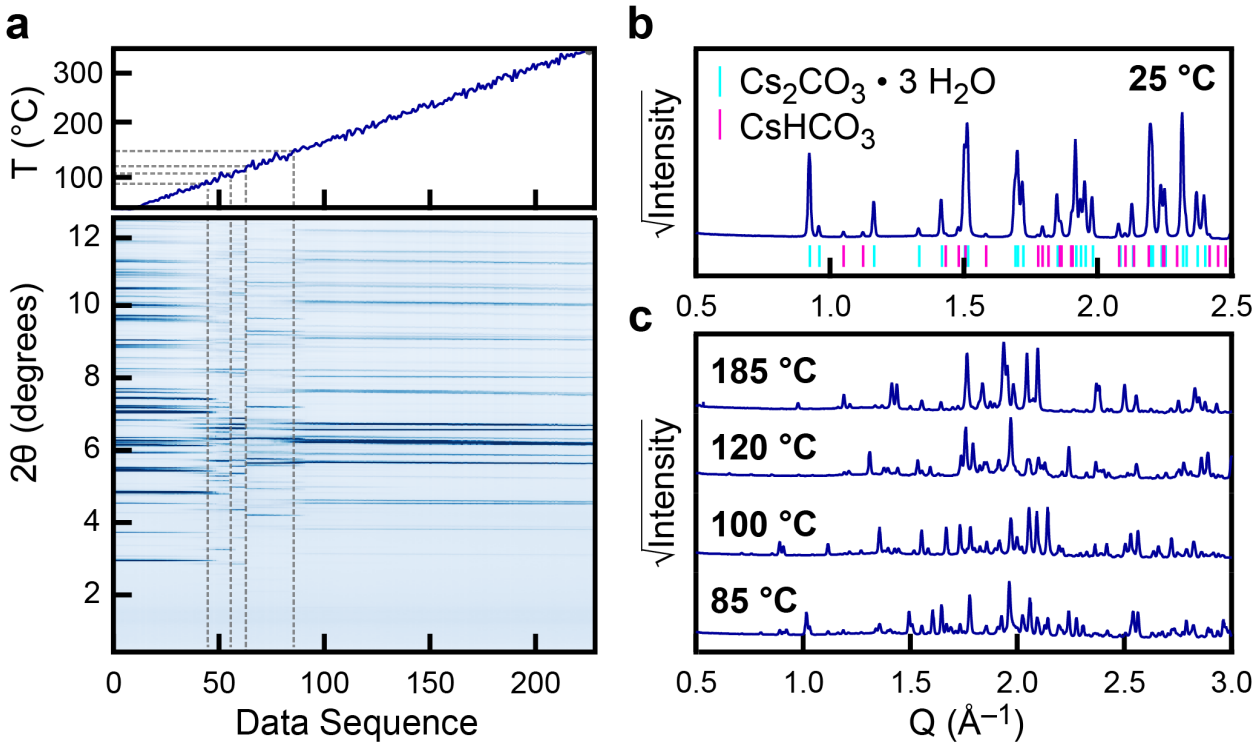

Figure S12 | Variable temperature PXRD of Cs_2CO_3. **a**, Temperature profile (top) and contour plot (bottom) of successive PXRD measurements collected while heating a sample of Cs_2CO_3 under 5 sccm He. Diffraction images were collected with $\lambda = 0.35488$ Å every 30 s while heating with a setpoint ramp rate of 3 °C min^{-1}. Diffraction intensity in the contour plot increases from white to blue. **b**, Ambient temperature PXRD pattern of Cs_2CO_3. Reference peak positions were obtained from the ICSD.[12,13] Though Cs_2CO_3 was purchased as an anhydrous salt, at room temperature the crystalline solid exists almost exclusively in its trihydrate form, with a small bicarbonate impurity. **c**, Individual elevated temperature PXRD patterns of the Cs_2CO_3 sample from the corresponding regions of the contour plot. While Cs_2CO_3 undergoes many phase transitions due to water loss while heating, it reaches its anhydrous form well below the temperatures at which furoate carboxylation is performed.

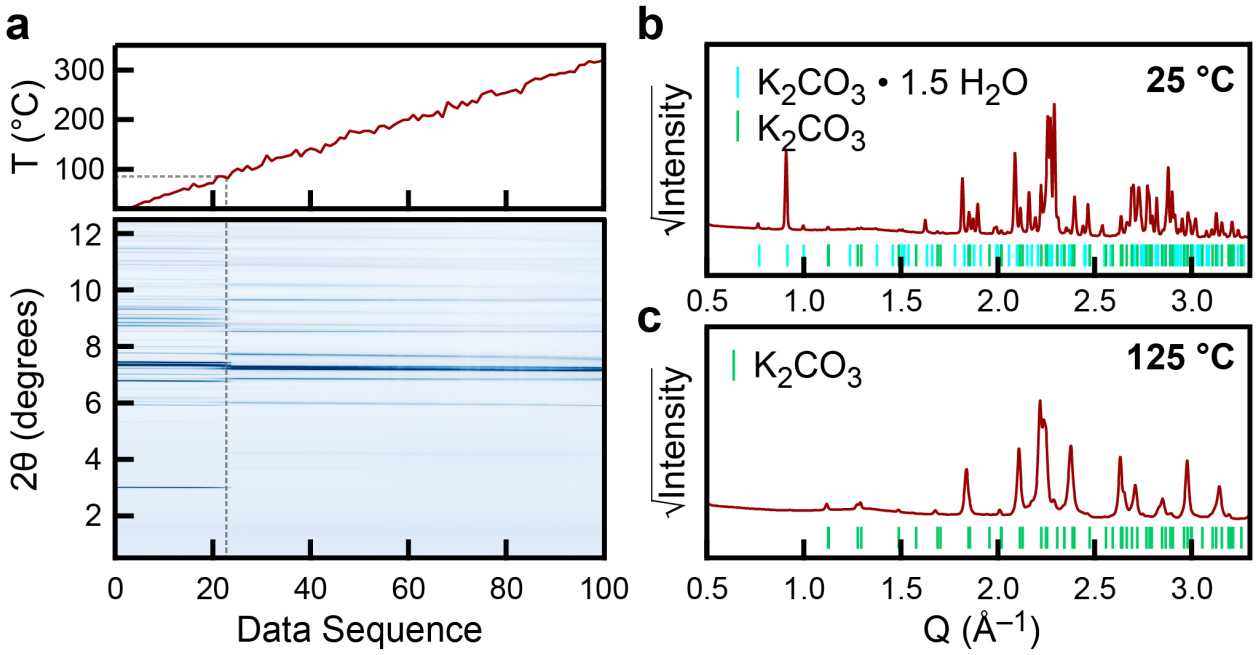

Figure S13 | Variable temperature PXRD of K_2CO_3. **a**, Temperature profile (top) and contour plot (bottom) of successive PXRD measurements collected while heating a sample of K_2CO_3 under 5 sccm He. Diffraction images were collected with $\lambda = 0.35488$ Å every 60 s while heating with a setpoint ramp rate of 3 °C min^{-1}. Diffraction intensity in the contour plot increases from white to blue. **b**, Ambient temperature PXRD pattern of K_2CO_3. Reference peak positions were obtained from the ICSD.[14,15] Though K_2CO_3 was purchased as an anhydrous salt, at room temperature the crystalline solid exists almost exclusively in its hydrate form. **c**, Elevated temperature PXRD pattern of K_2CO_3, confirming that the single observed phase transition corresponds to a dehydration event.

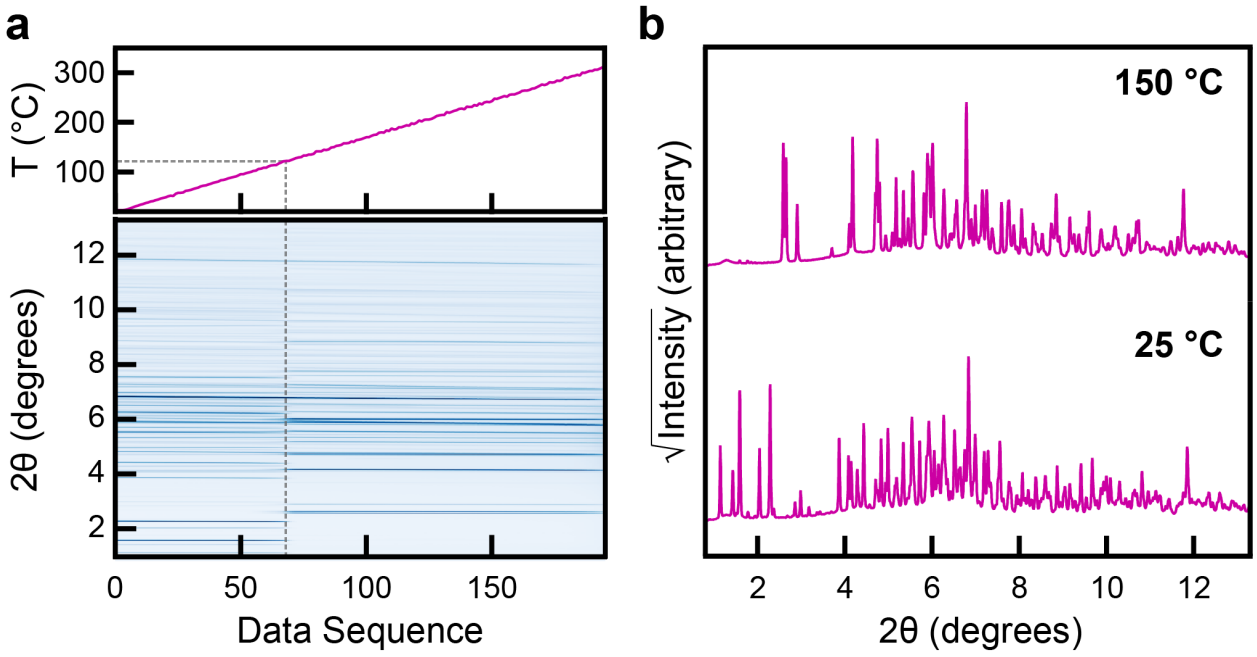

Figure S14 | Variable temperature PXRD of Cs_2FDCA. **a**, Temperature profile (top) and contour plot (bottom) of successive PXRD measurements collected while heating a sample of Cs_2FDCA under 5 sccm He. Diffraction images were collected with $\lambda = 0.34753$ Å every 30 s while heating with a setpoint ramp rate of 3 °C min^{-1}. Diffraction intensity in the contour plot increases from white to blue. **b**, Individual PXRD patterns for Cs_2FDCA at ambient and elevated temperature selected from the corresponding regions of the contour plot. Cs_2FDCA undergoes one phase transition while heating, assigned to dehydration of a crystalline salt hydrate. The salt reaches its elevated temperature anhydrous form well below the temperatures at which furoate carboxylation is performed, however, and remains stable in this solid phase up to temperatures >300 °C with no evidence of melting.

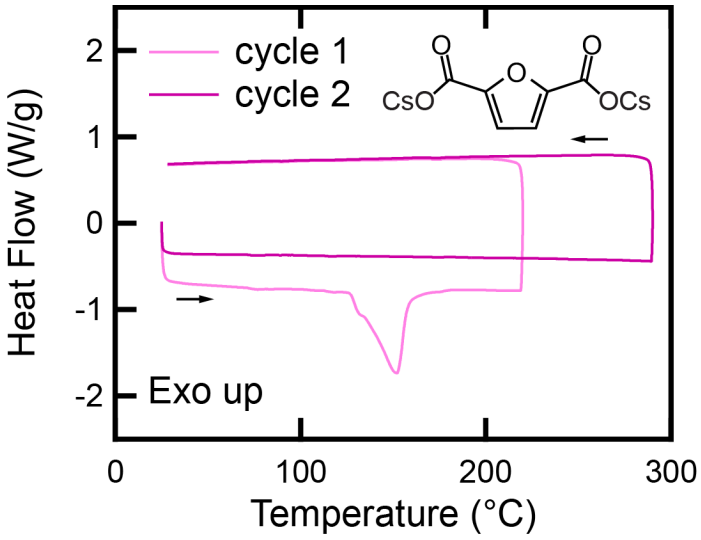

Figure S15 | Differential Scanning Calorimetry of Cs_2FDCA. Cs_2FDCA shows one irreversible endothermic event at T ~ 130 °C upon initial heating from room temperature, assigned to loss of water from a crystalline salt hydrate. No thermal events are observed in a second heating cycle following the removal of water.

3. References

1. Dick, G. R.; Frankhouser, A. D.; Banerjee, A.; Kanan, M.W. *Green Chem.* **2017**, *19*, 2966-2972.
2. Bruker, SAINT and SADABS, Bruker AXS Inc., Madison, WI, **2016**.
3. Sheldrick, G. M. *Acta Cryst.* **2015**, *A71*, 3-8.
4. Sheldrick, G. M. *Acta Cryst.* **2015**, *C71*, 3-8.
5. Dolomanov, O. V.; Bourhis, L. J.; Gildea, R. J.; Howard, J. A. K.; Puschmann, H. *J. Appl. Cryst.* **2009**, *42*, 339-341.
6. Chupas, P. J.; Chapman, K. W.; Kurtz, C.; Hanson, J. C.; Lee, P. L.; & Grey, C. P. *J. Appl. Cryst.* **2008**, *41* (4), 822–824.
7. Coelho, A. A. *TOPAS-Academic*, Version 6 (Coelho Software, **2016**).
8. Coelho, A. A. *J. Appl. Cryst.* **2003**, *36*, 86-95.
9. Dollase, W. A. *J. Appl. Cryst.* **1986**, *19*, 267-272.
10. Coelho, A. A. *J. Appl. Cryst.* 2**000**, *33*, 899-908.
11. Leclaire, A. *Journal of Solid State Chemistry* **2008**, *181*, 2338–2345.
12. Cirpus, V.; Wittrock, J.; Adam, A. *Z. anorg. allg. Chem.* **2001**, *627*, 533-538.
13. Kaduk, J. *Zeitschrift für Kristallographie – New Crystal Structures* **1993**, *205* (2), 319-320.
14. Idemoto, Y.; Richardson, J. W.; Koura, N.; Kohara, S.; Loong, C. *J. Phys. Chem. Solids* **1998**, *59* (3), 363-376.
15. Skakle, J. M. S.; Wilson, M.; Feldman, J. *Acta Cryst.* **2001**, *E57*, i94-i97.